Metal–Organic Frameworks

International Edition: DOI: 10.1002/anie.201507400
German Edition: DOI: 10.1002/ange.201507400

A Bio-inspired Approach for Chromophore Communication: Ligand-to-Ligand and Host-to-Guest Energy Transfer in Hybrid Crystalline Scaffolds

*Ekaterina A. Dolgopolova, Derek E. Williams, Andrew B. Greytak, Allison M. Rice, Mark D. Smith, Jeanette A. Krause, and Natalia B. Shustova**

Abstract: *Efficient multiple-chromophore coupling in a crystalline metal–organic scaffold was achieved by mimicking a protein system possessing 100% energy-transfer (ET) efficiency between a green fluorescent protein variant and cytochrome b_{562}. The two approaches developed for ET relied on the construction of coordination assemblies and host–guest coupling. Based on time-resolved photoluminescence measurements in combination with calculations of the spectral overlap function and Förster radius, we demonstrated that both approaches resulted in a very high ET efficiency. In particular, the observed ligand-to-ligand ET efficiency value was the highest reported so far for two distinct ligands in a metal–organic framework. These studies provide important insights for the rational design of crystalline hybrid scaffolds consisting of a large ensemble of chromophore molecules with the capability of directional ET.*

Efficient energy utilization that could significantly affect the current energy landscape involves a number of challenges, including achieving energy transfer (ET) in a predesigned pathway. For example, to mimic the natural photosystem, possessing high efficiency of directional ET, an artificial system should rely on the cooperative work of hundreds of chromophores. Owing to the complexity of the hierarchical chromophore organization, self-assembly typically becomes a key strategy to design ensembles with efficient ET, mimicking the natural analogues. Coordination polymers possessing well-defined rigid structures (for example, metal–organic frameworks (MOFs)) could potentially address the existing challenges in the modeling of long- and short-range ET processes.[1–18] A great advantage of these crystalline scaffolds is that the distances and angles between chromophores, as well as their molecular conformations, can be determined from single-crystal X-ray studies and controlled through the ligand design[20] or variation of the experimental conditions.[21–43] Previously, the synthetic and structural versatility of hybrid scaffolds was successfully deployed to design and study Dexter and Förster ET mechanisms.[1] However, development of the next generation of artificial systems possessing enhanced and directional ET still requires new structural insights.[1,12,44]

In designing the system presented here, we were inspired by the high ET efficiency achieved in a protein system (a "bio-inspired approach"): a didomain protein made from a green fluorescent protein variant (EGFP) and a heme-binding protein, cytochrome b_{562} (cyt b_{562}, Scheme 1).[19] Through modulation of chromophore coupling, Jones and co-workers showed that a rational design of the protein scaffold could lead to nearly 100% ET efficiency.[19] Herein, we focused on replication of the efficient multiple intermolecular chromo-

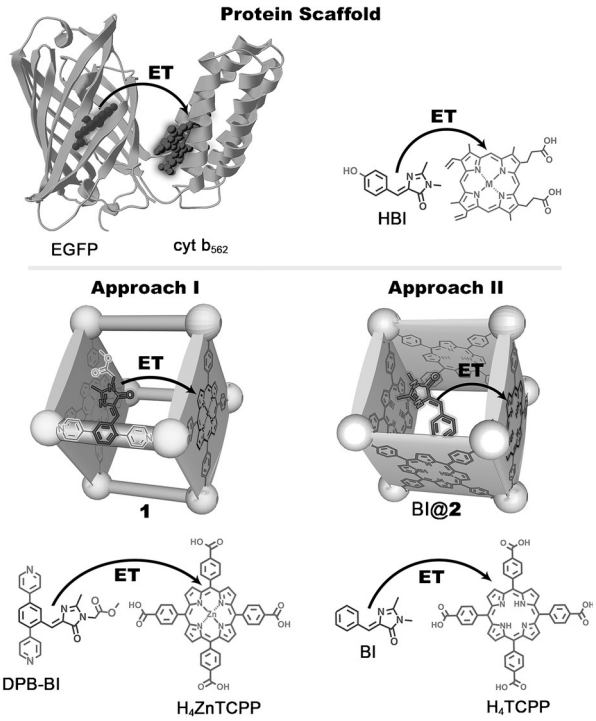

Scheme 1. (*top*) Representation of ET between the two coupled chromophore cores of a green fluorescent protein variant (EGFP) and the electron-transfer protein, cyt b_{562}.[19] (*bottom*) Approaches I and II involved incorporation of chromophores with HBI- and porphyrin-based cores inside the rigid scaffold. Approach I focused on coordinative immobilization of both chromophores in crystalline scaffolds **1** and **1′** while Approach II is based on inclusion of the BI donor in the porphyrin-based framework **2**.

[*] E. A. Dolgopolova, D. E. Williams, Prof. Dr. A. B. Greytak, A. M. Rice, Dr. M. D. Smith, Prof. Dr. N. B. Shustova
Department of Chemistry and Biochemistry, University of South Carolina
631 Sumter street, Columbia, SC 29208 (USA)
E-mail: shustova@sc.edu
Dr. J. A. Krause
Department of Chemistry, University of Cincinnati
Cincinnati, OH 45221 (USA)

Supporting information for this article is available on the WWW under http://dx.doi.org/10.1002/anie.201507400.

phore coupling achieved in the protein system through integration of chromophores with 4-hydroxybenzylidene imidazolinone (HBI) and porphyrin cores into an artificial rigid framework (Scheme 1). Recently, we showed that a porous MOF could be utilized as a mimic of the GFP β-barrel to maintain emission of HBI-based chromophores, and, therefore, replicate the photophysical properties of natural GFP-like systems.[46] In the present study, we designed multiple-chromophore hybrid scaffolds for modeling ET processes. The choice of chromophores with HBI and porphyrin cores was dictated by the necessary overlap of the emission spectrum of the donor (HBI-based derivative) with the absorption spectrum of the acceptor (porphyrin-based chromophore), which is required to accomplish efficient resonance energy transfer (RET). With this in mind, we prepared donor–acceptor pairs and developed two distinct approaches to achieve chromophore coupling through their incorporation into a rigid hybrid matrix (Scheme 1). Approach I involved coordinative immobilization of methyl-2-(4-(2,5-di(pyridin-4-yl)benzylidene)-2-methyl-5-oxo-4,5-dihydro-1*H*-imidazol-1-yl)acetate (DPB-BI, donor; Supporting Information, Figure S1) and tetrakis(4-carboxyphenyl)-porphyrin (H_4TCPP, acceptor), which resulted in formation of the crystalline MOFs. Approach II focused on non-coordinative inclusion of benzylidene imidazolinone (BI; Supporting Information, Figure S2) molecules (donor) inside a three-dimensional (3D) porphyrin-based host (acceptor). The guest size, host aperture, and chromophore photoluminescence (PL) responses were the main selection criteria in Approach II to achieve efficient chromophore coupling. To the best of our knowledge, the ligand-to-ligand ET efficiency (65%), calculated based on the experimental time-resolved PL data, is the highest value achieved so far between two distinct linkers in a MOF matrix.

In Approach I, incorporation of DPB-BI and H_4TCPP ligands into a rigid scaffold was achieved using a stepwise procedure. The four-step synthesis and molecular structure of the novel DPB-BI ligand utilized in scaffold preparation is described in the Supporting Information (Scheme S1, Figures S1, S3, S4). The first step of Approach I was preparation of a two-dimensional Zn_2(ZnTCPP) framework (Figure 1).[29] Afterwards, coordinative immobilization of DPB-BI was carried out through immersion of the Zn_2(ZnTCPP) crystals into *N*,*N*-dimethylformamide (DMF) or *N*,*N*-diethylformamide (DEF) solutions of DPB-BI (Supporting Information). Depending on the solvent choice in the second step, formation of two MOFs, $[Zn_2(ZnTCPP)(DPB\text{-}BI)_{0.86}\text{-}(DMF)_{1.14}]\cdot(DMF)_{8.86}(H_2O)_{20}$ (**1**) and $[Zn_2(ZnTCPP)(DPB\text{-}BI)_{0.64}(DEF)_{0.36}]\cdot(DEF)_{6.94}\cdot(H_2O)_{12.55}$ (**1′**), were achieved (Figure 1). In Approach II (Scheme 1), solvothermally prepared Pb_2(TCPP)·4DMF (**2**)[47] (Figure 2; Supporting Information, Figure S7) was soaked in the BI solution for 3 days, which resulted in BI inclusion and formation of BI@**2**. The frameworks **1, 1′**, and BI@**2** underwent comprehensive characterization by single-crystal and powder X-ray crystallography, elemental and thermogravimetric analyses, and FT-IR spectroscopy (Figures 1,2; Supporting Information, Figures S5–S14). Furthermore, the digested **1**, **1′**, and BI@**2** samples (destroyed in the presence of acid) were analyzed by mass-spectrometry and ^{1}H NMR spectroscopy (Supporting Information, Figures S15–S17).

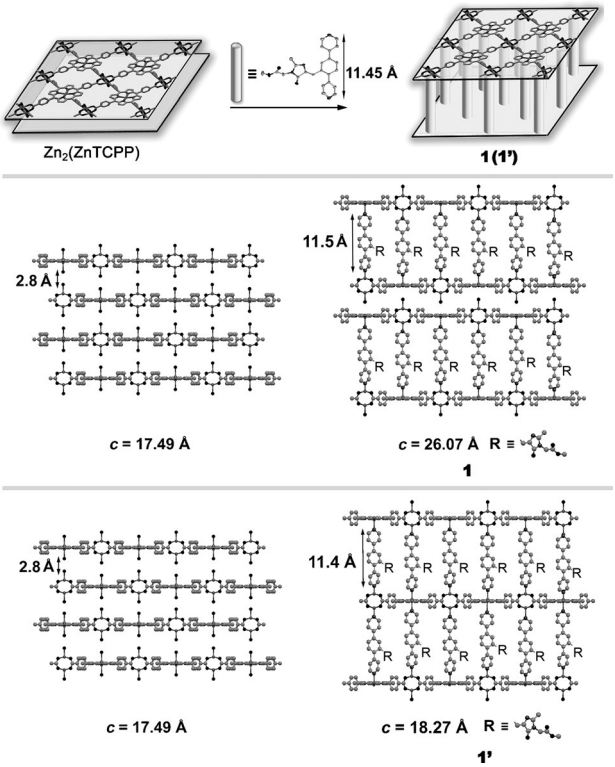

Figure 1. The X-ray structures of Zn_2(ZnTCPP),[45] DPB-BI, **1**, and **1′**. Increase of the interlayer distance occurred, owing to coordinative immobilization of DPB-BI.

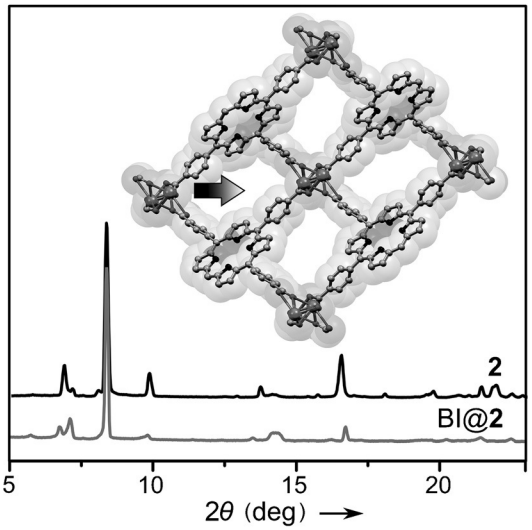

Figure 2. PXRD patterns of **2** and BI@**2**. The inset shows the single-crystal X-ray structure of **2**. The grey arrow indicates the 1D channels suitable for BI incorporation. H atoms and guest solvent molecules were omitted for clarity.

The structural analysis of **1** and **1′** is shown in Figure 1 (Supporting Information, Figures S5, S6). The Zn_2(ZnTCPP) framework consists of two-dimensional (2D) layers in which $ZnTCPP^{4-}$ is coordinated to paddle-wheel $Zn_2(O_2C\text{–})_4$ sec-

ondary building units (SBUs, Figure 1). Immersion of the 2D framework into a DPB-BI solution resulted in coordination of the second ligand by the replacement of the apical solvent molecules in the SBUs, and, thereby, formation of the crystalline scaffolds **1** and **1′**. The choice of solvent (DMF [**1**] versus DEF [**1′**]) used for DPB-BI immobilization affected the stacking of the 2D layers (Figure 1). In the case of **1**, DPB-BI connects pairs of 2D layers, while in **1′** DPB-BI connects all layers along the *c* axis. In both **1** and **1′**, DPB-BI insertion increased the interlayer distance by 2.8 Å (O···O distance in Zn_2(ZnTCPP)) to 11.5 Å (11.4 Å) (N···N distance in **1** (**1′**)), which is consistent with the DPB-BI length determined from its molecular structure (11.45 Å, Figure 1; Supporting Information, Figure S1). The powder X-ray diffraction (PXRD) studies of **1** and **1′** confirmed the preservation of crystallinity during the two-step chromophore immobilization procedure (Supporting Information, Figures S8, S9).

Structural analysis of **2** (Figure 2; Supporting Information, Table S1) revealed that the 3D framework utilized as a host for the BI molecules consists of $TCPP^{4-}$ linkers connected to carboxylate-bridged Pb^{2+} chains.[47] More importantly, **2** contains 1D 8 × 11 Å channels suitable for BI incorporation (Figure 2). The PXRD analysis showed that inclusion of BI molecules does not affect the host crystallinity, and spectroscopic studies of digested BI@**2** revealed that the framework contains one guest molecule per two $TCPP^{4-}$ units (Figure 2; Supporting Information, Figure S17).

To test whether ET can occur in the designed scaffolds, photophysical properties of donor/acceptor molecules as well as **1**, **1′**, and BI@**2** were studied by diffuse reflectance (DR), fluorescence, and time-resolved PL spectroscopies. For effective RET, the emission spectrum of the HBI-based donor should overlap with the absorption spectrum of the porphyrin-based acceptor. The absorption spectrum in the solid state was evaluated by DR (Figure 3a, b), and indicated the DPB-BI (donor) used for preparation of **1** is emissive in the range of 400–550 nm with λ_{max} = 440 nm (λ_{ex} = 365 nm). The BI molecule used in Approach II exhibits a similar PL profile to DPB-BI and emits in the same 400–550 nm range with λ_{max} = 440 nm (λ_{ex} = 365 nm, Figure 3c). Notably, the EGFP originally used in the didomain protein system (see above) fluoresces in the same range as BI and DPB-BI but with a slightly red-shifted emission maximum.[19] Therefore, the PL profiles of both BI and DPB-BI replicate the fluorescence response of the EGFP that was initially used as a model for the HBI-based chromophore design. Based on the DR data, both acceptors, Zn_2(ZnTCPP) and framework **2**, absorb light up to 650 nm (Figure 3a,c), which provides the necessary spectral overlap of their absorption profiles with the donor emission responses. Coordinative immobilization of both donor and acceptor moieties in rigid **1** and **1′** resulted in complete disappearance of donor emission (Figure 3, Supporting Information, Figure S18), which could be attributed to efficient ET.[7,48]

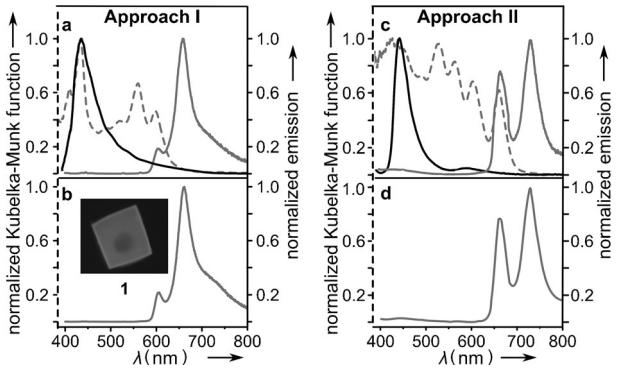

Figure 3. a) The DR spectrum of Zn_2(ZnTCPP) (dashed grey line) and emission spectra of DPB-BI (solid black line) and Zn_2(ZnTCPP) (solid grey line). b) The emission spectrum of **1**. The inset shows an epifluorescence microscopy image of a crystal of **1** (λ_{ex} = 510 nm). c) The DR spectrum of **2** (dashed grey line) and emission spectra of BI (solid black line) and **2** (solid grey line). d) The emission spectrum of BI@**2**. An excitation wavelength of 365 nm was used to acquire all PL spectra.

To quantitatively describe possible ET processes occurring in **1**, **1′**, and BI@**2**, time-resolved fluorescence decay measurements were carried out (Supporting Information, Figures S19–S21). The ET efficiency (Φ_{ET}) was determined based on donor lifetimes in the presence and absence of the acceptor molecules.[48] We investigated the PL decays within the donor emission range to exclude the PL response of porphyrin-based acceptors. Time-resolved decays for coordinatively immobilized DPB-BI (DPB-BI-**1** [or DPB-BI-**1′**], in the presence of the acceptor) and DPB-BI coordinated to Zn^{2+} (in the absence of the acceptor) demonstrated more rapid decay than free DPB-BI (Supporting Information, Figures S19, S20). Analysis of the curves with a reconvolution fit supported a triexponential decay model in each case and revealed a shortening of the amplitude-weighted average lifetimes from 1.09 (DPB-BI) to 0.38 and 0.51 ns in the presence of the acceptor molecules in **1** and **1′**, respectively (Table 1).

The estimated values of the corresponding Φ_{ET} and ET rate constant (k_{ET}) of **1** were found to be 65% and 1.71 × 10^{10} s^{-1}, respectively. Interestingly, slightly smaller Φ_{ET} (53%) was observed for **1′** (Table 1), which could be attributed to the different topology of **1′**, that is, the difference in stacking of 2D layers as shown in Figure 1. Notably, the excitation spectrum of **1**, obtained by scanning from 380 to 540 nm with fixed emission at 680 nm (PL from Zn_2(ZnTCPP)) is different from the excitation spectrum of Zn_2(ZnTCPP) (without DPB-BI immobilization; Supporting Information, Figure S22). Thus, the PL studies confirm that efficient ET from DPB-BI to Zn_2(ZnTCPP) takes place in the prepared

Table 1: The amplitude-weighted average lifetimes ($\langle\tau_{av}\rangle$), ET rate constants (k_{ET}), Förster critical radii (R_o), ET efficiency (Φ_{ET}), and spectral overlap functions (J) for DPB-BI, DPB-BI-**1**, DPB-BI-**1′**, BI, and BI@**2** samples.

	DPB-BI	DPB-BI-**1**	DPB-BI-**1′**	BI	BI@**2**
$\langle\tau_{av}\rangle$ [ns][a]	1.09	0.38	0.51	1.89	0.53
k_{ET} [× 10^{10} s^{-1}]	–	1.71	1.04	–	1.36
R_o [Å]	–	23	23	–	21
Φ_{ET} [%]	–	65	53	–	72
J [× 10^{-14} cm^3 M^{-1}]	–	6.25	6.25	–	4.57

[a] Detailed information relative to fitting of PL decays can be found in the Supporting Information.

scaffolds. Furthermore, to address the possibility of RET in **1** (**1′**), the Förster critical radius (R_o) was obtained through calculation of the spectral overlap function (J) and was found to be $J = 6.25 \times 10^{-14}\ cm^3 M^{-1}$ (Table 1; Supporting Information, Figure S23). On the basis of the calculated spectral overlap function, we estimated R_o to be 23 Å (Supporting Information, Figure S23), which is far beyond the donor–acceptor distance approximated from the structural data (the distance between Zn in the ZnTCPP unit and the corresponding N···N centroid of DPB-BI is roughly 7.7 Å). Thus, based on a combination of PL measurements and calculations of J and R_o, we attribute the observed changes in donor emission profile after its coordinative immobilization to RET.

A similar tendency was observed in the case of time-resolved studies of BI@**2**. The time-resolved PL decay of BI@**2** decreases more rapidly in comparison with the one acquired from a non-incorporated BI molecule (in the absence of acceptor **2**; Supporting Information, Figure S21). Similar to Approach I, the amplitude-weighted average lifetime in the presence of the acceptor (**2**) was found to be 0.53 ns, which is 3.5 times shorter in comparison to that determined for the non-incorporated BI chromophore (1.89 ns). Estimated Φ_{ET} in BI@**2** was found to be 72%. Thus, high Φ_{ET} values were achieved in both developed approaches. The estimated J for BI@**2** and the corresponding R_o were found to be $J = 4.57 \times 10^{-14}\ cm^3 M^{-1}$ and 21 Å, respectively (Supporting Information, Figure S23). Taking into account the dimensions of the 1D channels in **2** and the size of the incorporated BI molecules, the estimated R_o is far beyond the guest–host distance. Therefore, similar to **1** and **1′**, we attribute the changes in the time-resolved PL decays observed for the BI@**2** scaffold to RET.

To summarize, we have developed two distinct approaches focused on mimicking a protein system that possesses high ET efficiency. Moreover, both selected HBI-based chromophores, BI and DPB-BI, were emissive in the same range as the EGFP used in the targeted protein system. Combination of time-resolved PL studies with spectral overlap function calculations revealed high Φ_{ET} was achieved by coordinative immobilization of the donor/acceptor chromophores and non-coordinative inclusion of the donor molecules inside the acceptor scaffold. Furthermore, the experimental Φ_{ET} obtained through a rational design of **1**, based on the time-resolved PL data, is the highest value for ligand-to-ligand ET efficiency reported so far for MOFs. Thus, the bio-inspired approach demonstrated herein could foreshadow the utilization of hybrid scaffolds to direct chromophore behavior in large light-harvesting ensembles and, therefore, achieve directional energy transfer in a predesigned pathway.

Experimental Section

Full experimental details, time-resolved PL data, and theoretical calculations can be found in the Supporting Information. CCDC 1402130, 1402131, 1402132, 1402133, and 1421267 (2,5-di(pyridin-4-yl)benzaldehyde, DPB-BI, **1**, **2**, and BI) contain the supplementary crystallographic data for this paper. These data can be obtained free of charge from The Cambridge Crystallographic Data Centre.

Acknowledgements

This work was partially supported by the ASPIRE-I and III awards granted by the USC Office of the Vice President for Research. Crystallographic data were collected through the Service Crystallography at Advanced Light Source Program at beamline 11.3.1 at the Advanced Light Source (ALS), Lawrence Berkeley National Laboratory. The ALS is supported by the U.S. Department of Energy, Office of Basic Energy Sciences, Materials Sciences Division, under Contract DE-AC02-05CH11231.

Keywords: coordination polymers · energy transfer · fluorescence · green fluorescent protein · metal–organic frameworks

How to cite: *Angew. Chem. Int. Ed.* **2015**, *54*, 13639–13643
Angew. Chem. **2015**, *127*, 13843–13847

[1] T. Zhang, W. Lin, *Chem. Soc. Rev.* **2014**, *43*, 5982–5993.
[2] H.-J. Son, S. Jin, S. Patwardhan, S. J. Wezenberg, N. C. Jeong, M. So, C. E. Wilmer, A. A. Sarjeant, G. C. Schatz, R. Q. Snurr, O. K. Farha, G. P. Wiederrecht, J. T. Hupp, *J. Am. Chem. Soc.* **2013**, *135*, 862–869.
[3] K. Leong, M. E. Foster, B. M. Wong, E. D. Spoerke, D. Van Gough, J. C. Deaton, M. D. Allendorf, *J. Mater. Chem. A* **2014**, *2*, 3389–3398.
[4] D. E. Williams, J. A. Rietman, J. M. Maier, R. Tan, A. B. Greytak, M. D. Smith, J. A. Krause, N. B. Shustova, *J. Am. Chem. Soc.* **2014**, *136*, 11886–11889.
[5] C. A. Kent, B. P. Mehl, L. Ma, J. M. Papanikolas, T. J. Meyer, W. Lin, *J. Am. Chem. Soc.* **2010**, *132*, 12767–12769.
[6] C. A. Kent, D. Liu, L. Ma, J. M. Papanikolas, T. J. Meyer, W. Lin, *J. Am. Chem. Soc.* **2011**, *133*, 12940–12943.
[7] C. Y. Lee, O. K. Farha, B. J. Hong, A. A. Sarjeant, S. T. Nguyen, J. T. Hupp, *J. Am. Chem. Soc.* **2011**, *133*, 15858–15861.
[8] S. Jin, H.-J. Son, O. K. Farha, G. P. Wiederrecht, J. T. Hupp, *J. Am. Chem. Soc.* **2013**, *135*, 955–9588.
[9] C. A. Kent, D. Liu, A. Ito, T. Zhang, M. K. Brennaman, T. J. Meyer, W. Lin, *J. Mater. Chem. A* **2013**, *1*, 14982–14989.
[10] C. A. Kent, D. Liu, T. J. Meyer, W. Lin, *J. Am. Chem. Soc.* **2012**, *134*, 3991–3994.
[11] X. Zhang, W. Wang, Z. Hu, G. Wang, K. Uvdal, *Coord. Chem. Rev.* **2015**, *284*, 206–235.
[12] M. C. So, G. P. Wiederrecht, J. E. Mondloch, J. T. Hupp, O. K. Farha, *Chem. Commun.* **2015**, *51*, 3501–3510.
[13] J. Yu, Y. Cui, C.-D. Wu, Y. Yang, B. Chen, G. Qian, *J. Am. Chem. Soc.* **2015**, *137*, 4026–4029.
[14] J. Park, D. Feng, S. Yuan, H.-C. Zhou, *Angew. Chem. Int. Ed.* **2015**, *54*, 430–435; *Angew. Chem.* **2015**, *127*, 440–445.
[15] T. H. Noh, H. Lee, J. Jang, O.-S. Jung, *Angew. Chem. Int. Ed.* **2015**, *54*, 9284–9288; *Angew. Chem.* **2015**, *127*, 9416–9420.
[16] V. M. Suresh, S. J. George, T. K. Maji, *Adv. Funct. Mater.* **2013**, *23*, 5585–5590.
[17] D. Yan, Y. Tang, H. Lin, D. Wang, *Sci. Rep.* **2014**, *4*, 4337.
[18] C. Gu, N. Huang, F. Xu, J. Gao, D. Jiang, *Sci. Rep.* **2015**, *5*, 8867.
[19] J. A. J. Arpino, H. Czapinska, A. Piasecka, W. R. Edwards, P. Barker, M. J. Gajda, M. Bochtler, D. D. Jones, *J. Am. Chem. Soc.* **2012**, *134*, 13632–13640.
[20] Y. Hong, J. W. Y. Lam, B. Z. Tang, *Chem. Soc. Rev.* **2011**, *40*, 5361–5388.
[21] H. Furukawa, K. E. Cordova, M. O'Keeffe, O. M. Yaghi, *Science* **2013**, *341*, 1230444.
[22] S. Furukawa, J. Reboul, S. Diring, K. Sumida, S. Kitagawa, *Chem. Soc. Rev.* **2014**, *43*, 5700–5734.

[23] M. L. Foo, R. Matsuda, S. Kitagawa, *Chem. Mater.* **2014**, *26*, 310 – 322.
[24] S. S. Nagarkar, B. Joarder, A. K. Chaudhari, S. Mukherjee, S. K. Ghosh, *Angew. Chem. Int. Ed.* **2013**, *52*, 2881 – 2885; *Angew. Chem.* **2013**, *125*, 2953 – 2957.
[25] S. M. Cohen, *Chem. Rev.* **2012**, *112*, 970 – 1000.
[26] A. Schaate, P. Roy, T. Preusse, S. J. Lohmeier, A. Godt, P. Behrens, *Chem. Eur. J.* **2011**, *17*, 9320 – 9325.
[27] C. Kutzscher, H. C. Hoffmann, S. Krause, U. Stoeck, I. Senkovska, E. Brunner, S. Kaskel, *Inorg. Chem.* **2015**, *54*, 1003 – 1009.
[28] B. Manna, S. Singh, A. Karmakar, A. V. Desai, S. K. Ghosh, *Inorg. Chem.* **2015**, *54*, 110 – 116.
[29] L. E. Kreno, K. Leong, O. K. Farha, M. Allendorf, R. P. Van Duyne, J. T. Hupp, *Chem. Rev.* **2012**, *112*, 1105 – 1125.
[30] Z.-M. Zhang, T. Zhang, C. Wang, Z. Lin, L.-S. Long, W. Lin, *J. Am. Chem. Soc.* **2015**, *137*, 3197 – 3200.
[31] M. Tu, S. Wannapaiboon, R. A. Fischer, *Inorg. Chem. Front.* **2014**, *1*, 442 – 463.
[32] K. C. Stylianou, R. Heck, S. Y. Chong, J. Bacsa, J. T. A. Jones, Y. Z. Khimyak, D. Bradshaw, M. J. Rosseinsky, *J. Am. Chem. Soc.* **2010**, *132*, 4119 – 4130.
[33] M. D. Hill, S. El-Hankari, M. Chiacchia, G. J. Tizzard, S. J. Coles, D. Bradshaw, J. A. Kitchen, T. D. Keene, *Cryst. Growth Des.* **2015**, *15*, 1452 – 1459.
[34] S. B. Aliev, D. G. Samsonenko, M. I. Rakhmanova, D. N. Dybtsev, V. P. Fedin, *Cryst. Growth Des.* **2014**, *14*, 4355 – 4363.
[35] Q.-Y. Yang, M. Pan, S.-C. Wei, K. Li, B.-B. Du, C.-Y. Su, *Inorg. Chem.* **2015**, *54*, 5707 – 5716.
[36] J. Heine, K. Müller-Buschbaum, *Chem. Soc. Rev.* **2013**, *42*, 9232 – 9242.
[37] D. Yan, G. O. Lloyd, A. Delori, W. Jones, X. Duan, *Chempluschem* **2012**, *77*, 1112 – 1118.
[38] C.-Y. Sun, X.-L. Wang, X. Zhang, C. Qin, P. Li, Z.-M. Su, D.-X. Zhu, G.-G. Shan, K.-Z. Shao, H. Wu, J. Li, *Nat. Commun.* **2013**, *4*, 2717.
[39] Y. Tang, W. He, Y. Lu, J. Fielden, X. Xiang, D. Yan, *J. Phys. Chem. C* **2014**, *118*, 25365 – 25373.
[40] Y. Cui, Y. Yue, G. Qian, B. Chen, *Chem. Rev.* **2012**, *112*, 1126 – 1162.
[41] Y. Xiao, Y. Cui, Q. Zheng, S. Xiang, G. Qian, B. Chen, *Chem. Commun.* **2010**, *46*, 5503 – 5505.
[42] D. F. Sava, L. E. S. Rohwer, M. A. Rodriguez, T. M. Nenoff, *J. Am. Chem. Soc.* **2012**, *134*, 3983 – 3986.
[43] D. F. Sava Gallis, L. E. S. Rohwer, M. A. Rodriguez, T. M. Nenoff, *Chem. Mater.* **2014**, *26*, 2943 – 2951.
[44] A. L. Ortiz, G. S. Collier, D. M. Marin, J. A. Kassel, R. J. Ivins, N. G. Grubich, M. G. Walter, *J. Mater. Chem. C* **2015**, *3*, 1243 – 1249.
[45] B. J. Burnett, W. Choe, *CrystEngComm* **2012**, *14*, 6129 – 6131.
[46] D. E. Williams, E. A. Dolgopolova, P. J. Pellechia, A. Palukoshka, T. J. Wilson, R. Tan, J. M. Maier, A. B. Greytak, M. D. Smith, J. A. Krause, N. B. Shustova, *J. Am. Chem. Soc.* **2015**, *137*, 2223 – 2226.
[47] C. Zou, M.-H. Xie, G.-Q. Kong, C.-D. Wu, *CrystEngComm* **2012**, *14*, 4850 – 4856.
[48] J. R. Lakowicz, *Principles of Fluorescence Spectroscopy Principles of Fluorescence Spectroscopy*, Springer, Heidelberg, **2007**.

Received: August 8, 2015
Published online: September 17, 2015

